# Liquid Holdup in Rotating Packed Beds: Examination of the Film Flow Assumption

**Andjelko Bašić and Milorad P. Duduković**
Chemical Reaction Engineering Lab., Washington University, St. Louis, MO 63130

*Possibilities of predicting liquid holdup in rotating packed beds are examined using the film flow theory. A hydrodynamic model based on film flow on the particle scale accommodates both laminar and turbulent films in the entry and developed regime. Conductance measurement was used for experimental determination of liquid holdup and estimation of the degree of anisotropy of liquid distribution. Experimental results represent the first data for liquid holdup in the rotating packed bed as a function of operating conditions and liquid properties. They indicate an anisotropic liquid distribution dependent on the operating variables. While the film model can be fitted to the experimental data, such a fit lacks a theoretical basis and the classical theory of film flow on the particle scale cannot explain the liquid flow in rotating packed beds. An empirical expression correlates well the holdup data with the operating parameters.*

## Introduction

Rotating packed beds (RPB) were introduced as gas-liquid contactors to increase mass-transfer rates between the phases, above those achievable in standard packed beds (Ramshaw and Mallinson, 1981). Mass-transfer performance is improved by replacing gravity with centrifugal force as the driving force for liquid flow; because centrifugal acceleration can be many times higher than gravitational, the rotating packed bed was named HIGEE, an acronym for "high $g$."

Figure 1 shows the cross section of the RPB unit used in our laboratory. This design was needed to meet the requirements of the previous mass-transfer study (Munjal, 1989b). (Commercial RPBs are usually of the simple design, in which the rotor is without the side wall, and gas is introduced from the casing space (10). This eliminates the need for a hollow drive shaft (2), gas nozzles (12), and liquid seal, (9).) The path of gas and liquid in Figure 1 shows that the flow in the packed section of the RPB is analogous to that in conventional packed beds with countercurrent gas-liquid flow. However, volumetric gas-liquid mass-transfer coefficients achievable in the RPB are one to two orders of magnitude higher than in conventional packed beds (Ramshaw and Mallinson, 1981). Furthermore, flooding occurs at higher values of gas and liquid flow rate (Ramshaw, 1983) allowing higher capacity, so that a much smaller RPB than a conventional packed bed is needed for a given operation.

In spite of these advantages, RPB has been used little in industry, mostly in separation operations (Fowler, 1989), probably because of practitioners' preference for conventional packed beds without moving parts. The real advantage of RPBs for potential future use is for processes in which mass transfer is just one, but the critical step. For example, high mass-transfer rate recommends the RPB as gas-liquid reactor for systems with high reaction rates, but with mass-transfer limitations in conventional equipment. Short residence time of the liquid could be exploited in reacting systems with selectivity requirements, high centrifugal force for processing of non-Newtonian fluids or very viscous newtonian fluids (such as stripping monomers or solvents from polymers), for operation in microgravity, and so on.

The following list of the RPB literature is to our knowledge complete. Vivian et al. (1965) were the first to address the dependence of mass-transfer rates on a variable body force by measuring the gas-liquid mass-transfer coefficient in a packed bed mounted at the end of a rotating arm. Using limited data they concluded that liquid-side mass-transfer coefficient was proportional to overall acceleration raised to the power of 0.41 or 0.48, depending on the liquid flow rate. Tung and Mah

Present address of A. Bašić: Laboratorium voor Chemische Technologie, Eindhoven University of Technology, P.O. Box 513, 5600 MB Eindhoven, The Netherlands.

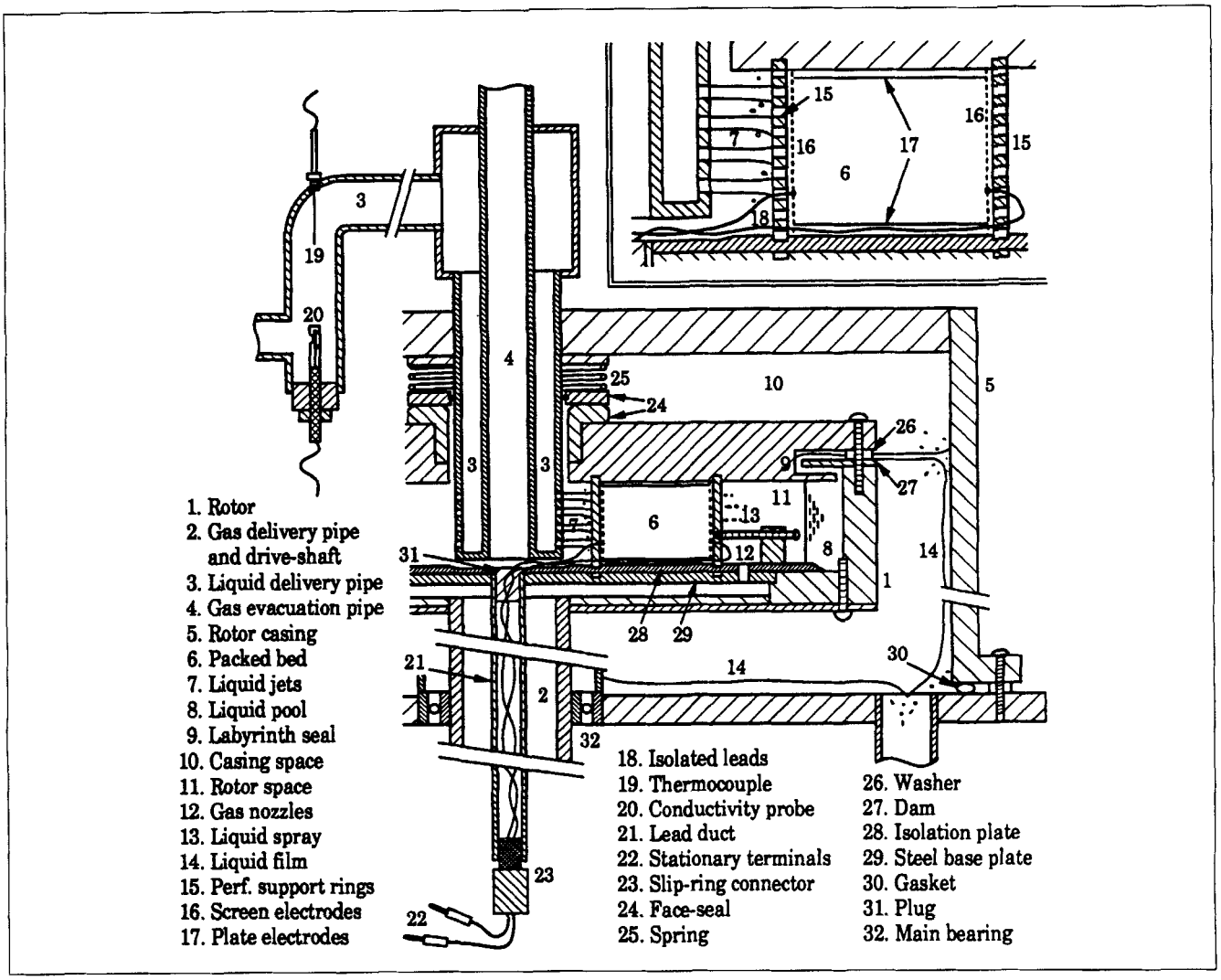


**Figure 1. RPB for countercurrent operation.**

Main rotating parts: (1) and (2). Main stationary parts: (3), (4) and (5). Liquid path: from pipe (3) to (stationary) jets (7), to (rotating) packed section (6), to (rotating) liquid pool (8) and out through liquid seal (9). Gas path: from pipe (2) through nozzles (12) into space (11), and by $p$-difference across bed (6) to (stationary) pipe (4).

(1985) proposed a formula for the liquid-side gas-liquid mass-transfer coefficient based on a theoretical expression for absorption rate in hydrodynamically developed laminar liquid films and on an empirical correlation for the gas-liquid interfacial area in conventional packed beds. The agreement with experimental results of Ramshaw and Mallinson (1981) was fair. Mersmann et al. (1986) presented an overview of various mass-transfer devices employing centrifugal force and compared their performance estimated by generalized empirical relationships. Munjal et al. (1989a,b) reported data for the liquid-side gas-liquid mass-transfer coefficient, gas-liquid interfacial area and gas-solid mass-transfer coefficient. Further, they proposed a model of mass transfer based on developed laminar films and complete wetting of the packing. The agreement between the experimental results and the model suggests that the assumptions about liquid flow were not unreasonable. Keyvani and Gardner (1989) reported experimental results for the gas-liquid mass-transfer rates, pressure drop and liquid residence time distribution, and gave a comprehensive list of industrial applications of RPBs. Kumar and Rao (1990) compared experimental data for the liquid-side gas-liquid mass-transfer coefficient to the correlation of Tung and Mah (1985) and found a poor agreement. They also presented results of pressure drop measurements over a limited range of operating conditions.

No experimental findings for liquid holdup have been reported so far, and our primary goal was to measure liquid holdup as a function of the operating conditions. These results should be of practical importance in new applications of RPB, because holdup determines the residence time of the liquid and thus the time available for completion of chemical reactions and of any other process with finite rate. The second goal was to predict liquid holdup using a model of liquid flow. For the basis of the model we selected the film flow assumption which has so far been used unverified in mass-transfer models (Tung and Mah, 1985; Munjal et al., 1989a,b). By comparing the model prediction of holdup to experimental results, we try to confirm or disprove the film flow assumption.

## Previous Studies

We summarize first the hydrodynamic models for conventional packed beds based on the film flow assumption. After that we show that holdup measurement based on electrical conductance was the only experimental method appropriate for the RPB and summarize the results of such measurements in conventional packed beds.

### *Models of holdup in conventional packed beds*

Hydrodynamic models of conventional packed beds based on liquid films were proposed by Davidson (1959), Buchanan (1967), Yilmaz and Brauer (1978), and Bemer and Kalis (1978). The premise of these models is that flow of liquid through a packed bed can be related to film flow over a single particle. In order to define a tractable problem on the particle scale, external particle surface is represented by a set of flat surfaces, called facets, joined to one another at end points to form a chain extending in the main flow direction. Physically, facets represent free surfaces of packing elements over which films may flow uninterrupted, and facet joints represent the points at which adjacent packing elements touch and the film is forced to change direction. To account for the irregularity of the packing surface, Davidson (1959) assigned random geometrical properties to facets. In all models liquid was assumed to be the only flowing phase, and its volume per unit volume of the packed bed was assumed to be given by:

$$\epsilon\beta = a_w \bar{h}. \tag{1}$$

$a_w$ denotes the specific wetted surface area of the packing, $\bar{h}$, the mean film thickness, $\epsilon$ the bed voidage, and $\beta$ liquid saturation of the voids, defined as the ratio of the liquid and the void volume. To predict liquid holdup, it is then necessary to describe the dependence of $a_w$ and $\bar{h}$ on the operating conditions. In all models, specific wetted area was either assumed equal to the specific packing area, $a_p$, or accounted for by empirical correlations. On the other hand, mean film thickness, $\bar{h}$, was found by solving the particle scale problem under different assumptions about the film flow. Figure 2 shows these assumptions, and we summarize next the resulting expressions for liquid holdup.

According to Davidson (1959) (Figure 2a) the flow is laminar and fully developed, and film thickness on every facet, $h$, is described by Nusselt's (1916) formula given in Table 1. The mean film thickness, $\bar{h}$, is obtained by averaging $h$ with respect to the assumed distribution of facet inclination, and the result for holdup is:

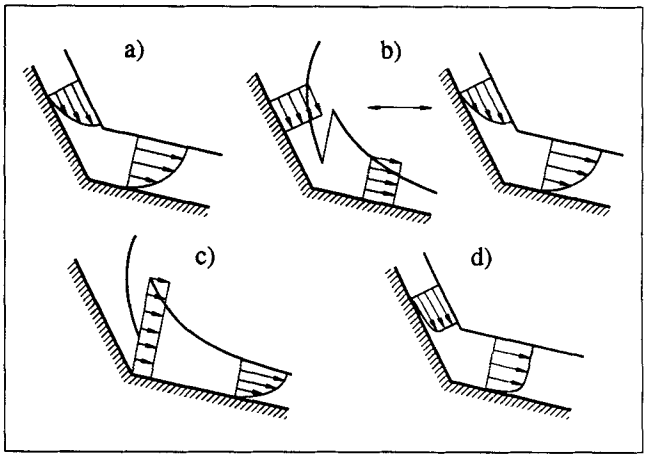


**Figure 2. Flow regimes assumed in hydrodynamic models of conventional packed beds.**

a) Davidson (1959), developed laminar flow and random facet inclination; b) Buchanan (1967), left—gravity-inertia regime (one-dimensional potential flow), right—gravity-viscosity regime (developed laminar flow); c) Yilmaz and Brauer (1973), developing laminar flow; d) Bemer and Kalis (1978), developed turbulent flow.

$$\epsilon\beta = a_w \bar{h} = 1.932 a_w d_p \left(\frac{Re}{Ga}\right)^{1/3}. \tag{2}$$

$Re$ denotes the film Reynolds number, $(\Gamma/\nu)$, with $\Gamma$ denoting liquid flow rate per unit width of the solid surface. $Ga$ denotes the Galileo number based on the size of the packing element, $d_p$, defined as $(g d_p^3/\nu^2)$. Davidson (1959) compared his prediction for $\bar{h}$ to the ratio of experimental data for holdup, $(\epsilon\beta)$, and for specific wetted area, $a_w$, and found them in agreement which may be called fair, considering that his model has no adjustable parameters.

Buchanan (1967) assumed that films on facets passed through different flow regimes as operating conditions were varied, and based his holdup prediction on the two limiting ones, called the gravity-inertia and the gravity-viscosity regime (Figure 2b). The gravity-inertia regime is in fact one-dimensional potential flow, which has been used in falling film hydrodynamics to model entry flow (such as Haugen, 1968; Andersson and Ytrehus, 1985), and the gravity-viscosity regime is just developed laminar flow. In the final form the expression for holdup is:

$$\epsilon\beta = 2.2(a_p d_p)^{1/3}\left(\frac{Re}{Ga}\right)^{1/3} + 1.8 a_p d_p Fr^{1/2}. \tag{3}$$

**Table 1. Values of Constants in the Correlation $h_a = B^{2/3}(\nu^2/g_x)^{1/3} Re^{2m/3}$**

| Reference | $B$ | $m$ | Reference | $B$ | $m$ |
|---|---|---|---|---|---|
| Nusselt (1916) (laminar) | $\sqrt{3}$ | 1/2 | Belkin et al. (1959) | 0.167 | 0.875 |
| Feind (1960) | 0.388 | 0.750 | Ganchev et al. (1974) | 0.171 | 0.875 |
| Takahama and Kato (1980) | 0.325 | 0.789 | Henstock and Hanratty (1976) | 0.132 | 0.900 |
| Brauer (1956) | 0.287 | 0.800 | Ueda and Tanaka (1974) | 0.109 | 0.945 |
| Gimbutis (1974); Gimbutis et al. (1978) | 0.179 | 0.874 | Brötz (1954) | 0.0713 | 1.000 |

The first term describes the gravity-viscosity and the second the gravity-inertia regime, $Fr$ denotes the Froude number defined as $\Gamma^2/(gd_p^3)$ and coefficients 2.2 and 1.8 are adjustable constants, of which the second incorporates a factor for the assumed energy loss at facet joints. Complete wetting of the packing was assumed by replacing $a_w$ in Eq. 1 by $a_p$. In a later work Buchanan (1988) noticed a discrepancy between Eq. 3 and some additional experimental data, ascribed it to incomplete wetting, and changed the exponents in order to achieve better agreement with the data.

Using numerical analysis of film flow on an incline and experimental results for film flow of other authors, Yilmaz and Brauer (1973) compiled a map of film flow regimes and argued that the flow on the assumed facets of a packed bed was always laminar (Figure 2c). Their correlation for holdup is based on the numerical solution for film thickness of a developing falling film, but its final form was modified to fit the experimental data:

$$\epsilon\beta = \{4Fr^2 + [1.044(a_p d_p)^{1.7127} Ga^{-0.4787} Ka^{-0.0477} Re^{0.563}]^2\}^{1/2}. \tag{4}$$

The Kapitza number, $Ka = \mu^4 g/(\sigma^3 \rho)$, (instead of which these authors use the reciprocal, $Ka^{-1}$, denoting it by $K$ and calling it *die Flüssigkeitskennzahl*), was introduced through an empirical formula for specific wetted area of Raschig rings.

Finally, Bemer and Kalis (1978) considered the developed flow of both laminar and turbulent films (Figure 2d). For the latter they used the formula:

$$\bar{h} = \left(\frac{f'}{2}\right)^{1/3} \left(\frac{\nu^2}{g}\right)^{1/3} Re^{2/3} \tag{5}$$

in which $f'$ is a constant with the physical meaning of friction factor. Assuming complete wetting, $a_w = a_p$, and adjusting the value of $f'$, these authors achieved a satisfactory agreement of the predicted and measured holdup. Their results suggest that films may be turbulent at values of $Re$ as low as ten.

### *Packed bed holdup through electrical conductance*

As it flows through the RPB liquid is retained in its different parts shown in Figure 1 (such as inlet pipe (3), jets (7), spray (13), and liquid pool (8), films on the casing walls (14), but only liquid in the voids of the packing, between the support rings (15) is of interest. The volume of this liquid, $(V_B \epsilon \beta_V)$, may well be smaller than the volume of liquid in other parts of the rotor by one to two orders of magnitude. For example, the volume of just the liquid making up the pool (8) is about twice as large as the volume of the entire packed section, $V_B (\sim 5 \times 10^{-4} \text{m}^3)$. Because of such a large liquid inventory outside of the packed section, only a measurement method which addresses the liquid in the packed section and effectively isolates liquid in other parts of the rotor can give meaningful results.

Standard measurement methods for liquid holdup in packed beds are draining (Larkins et al., 1961; Wammes et al., 1990) weighing (Crine and Marchot, 1981), closed loop (Charpentier et al., 1968) and tracer response (Dudukovic, 1986). These methods are direct in the sense that it is not necessary to use a model in order to obtain holdup from the result of the measurement. Unfortunately, there is no reasonably simple way to drain, weigh, or enclose in a flow loop or trace the packed section independently of the other parts of the rotor, and we could not take advantage of direct methods. This led us to the conductance method which allowed us to convert the holdup information into an electrical signal in the packed bed itself, avoiding the liquid in other parts of the rotor, and to bring it out of the rotor in the electrical form. To recover the holdup information we used a relationship between the bed conductance and holdup. We consider next such conductance-holdup models for conventional packed beds.

In packed beds, with liquid as the only conducting phase, the conductance method has often been used for describing local or time varying distribution of the liquid, or to determine parameters of a model of liquid distribution (Prost, 1967; Charpentier et al., 1968; Blok and Drinkenburg, 1982). However, when used in this way, conductance is not a source of information about steady-state liquid holdup of the whole bed. The only studies in which, to our knowledge, conductance of a packed bed was compared to independently measured holdup are those of Prost and Le Goff (1964) and Achwal and Stepanek (1975).

Achwal and Stepanek (1975) measured conductance of a bed filled with batch liquid and with gas passing in upward bubble flow. Measurements were made in the axial direction between single wire electrodes placed across the packing near the top and the bottom of the column. If by $R$ we denote bed resistance, by $S$ its reciprocal conductance and by indices $a$ and $f$ the axial (flow) direction and full saturation, respectively, the results of Achwal and Stepanek (1975) may be summarized by:

$$\frac{S_a}{S_{a,f}} = \frac{R_{a,f}}{R_a} = \beta, \tag{6}$$

which has a coefficient of correlation of 0.986 and standard deviation of 4%. Prost and Le Goff (1964) measured conductance in the axial direction using several aqueous solutions of different viscosity and surface tension as the liquid phase, and air as the gas phase, in both cocurrent and countercurrent flow. Normalized with conductance of the column filled only with liquid, $S_{a,l}$, and plotted against $(\epsilon\beta)$, their data for conductance with two-phases, $S_a$, follow a straight line:

$$\frac{S_a}{S_{a,l}} = \frac{R_{a,l}}{R_a} \propto \epsilon\beta. \tag{7}$$

These authors measured conductance also in the transverse direction by using two plate-electrodes fixed onto the column wall, one opposite the other. They correlated these results with those for axial direction and with holdup, using the expression:

$$\frac{S_t/S_{t,l}}{S_a/S_{a,l}} = \frac{R_{t,l}/R_t}{R_{a,l}/R_a} = \beta^{0.35}, \tag{8}$$

where index $t$ denotes the transverse direction. Prost and Le Goff (1964) explained their observations by a qualitative model according to which liquid forms rivulets extending in the axial direction and connected to some degree in the transverse direction. They suggested that the ratio of normalized conduc-

tances given by Eq. 8 could be used to quantify transverse "connectivity" and thus as a measurable parameter of the isotropy of liquid distribution.

## Film Flow Model of the RPB

Cylindrical symmetry and radial flow do not allow the same expressions for liquid holdup and saturation to be used for RPB as for conventional packed beds. We denote local liquid saturation of the voids by $\beta$ and assume it to depend only on the radial position. This assumption will be discussed shortly. Then, defining the overall liquid saturation of the packed section, $\beta_V$, as the ratio of the overall liquid volume and of the packed bed total void volume, we have:

$$\beta_V=\frac{1}{\epsilon V_B}\int_{V_B}\beta d(\epsilon V_B)=\frac{2}{r_o^2-r_i^2}\int_{r_i}^{r_o}r\beta dr. \tag{9}$$

$r_i$ and $r_o$ denote the inlet and the outlet bed radius, respectively, and the second equality follows under the additional assumption that porosity, $\epsilon$, is constant. Since it is proportional to the overall liquid volume of the RPB, we call $\beta_V$ the mean liquid saturation.

For model verification experimental measurements of the radial distribution of local saturation, $\beta(r)$, would be most useful, while from the practical point of view, data about the mean saturation, $\beta_V$, are needed. However, instead of either one of these, our method of measuring conductance in the radial direction (to be described later) gives only the radial saturation mean, $\langle\beta\rangle$, defined by:

$$\frac{1}{\langle\beta\rangle}=\frac{1}{\ln\frac{r_o}{r_i}}\int_{r_i}^{r_o}\frac{dr}{r\beta}, \tag{10}$$

Using numerical examples, we show in Appendix A that $\beta_V$ and $\langle\beta\rangle$ are close in value so that using the radial saturation mean, $\langle\beta\rangle$, as an approximation for the mean saturation, $\beta_V$, does not introduce an error much larger than the error of measurement, which as will be shown is small. Since, in addition, the radial saturation mean, $\langle\beta\rangle$, was found to be very sensitive to operating conditions and possible to measure with good accuracy and reproducibility, it provides a good basis for comparison of the model with experimental data.

### *Assumptions*

The starting assumption of the model is that liquid flows through the RPB in the form of films. We consider only film flow without capillary effects and assume the packing surface to be completely wetted:

$$a_w=a_p. \tag{11}$$

By this we limit the goal of the model to verifying whether liquid holdup can be predicted on the basis of film flow with complete wetting of the packing surface.

Other assumptions and their justifications are: (1) liquid is the only flowing phase, experimental results show this to be a good approximation, as far as holdup is concerned; (2) Coriolis and gravitational force may be neglected. Local saturation, $\beta$, is a function of the radius only. We show in Appendix B that these forces are of lesser magnitude than the centrifugal. Inasmuch as all forces except the centrifugal are neglected, the problem is one-dimensional and $\beta=\beta(r)$. (3) Packing surface may be represented by a chain of facets parallel to the $z$-axis and randomly inclined with respect to the radial direction. These facets, which we call rotating blades, are analogous to the facets of Davidson's (1959) model. Bašić (1992) showed that they were just one, but the most important type of facets that can be defined for the geometry of the RPB.

### *Film flow on the facet scale and liquid saturation*

The length of the rotating blade, $d_b$, corresponds to the length of the part of the packing element surface over which a film can flow uninterrupted. We set

$$d_b=\frac{d_p}{2}, \tag{12}$$

because in experiments we used glass spheres. For spheres in hexagonal close packing the length of the surface arc on one sphere, between two adjacent contact points with neighboring spheres, equals $\pi d_p/6\approx d_p/2$. We assumed blade inclination to the radial direction, $\theta$, to be a random variable with uniform probability distribution between 0 and $\pi/2$. Flow rate per unit width of the blade, $\Gamma$, is then given by (Davidson, 1959)

$$\Gamma=\frac{\pi}{2}\frac{(L/A_B)}{a_p}. \tag{13}$$

$A_B$ denotes the area of the bed section perpendicular to flow. For the RPB, this equals $(2r\pi H_B)$, and for the film Reynolds number, $Re$, we have

$$Re=\frac{\Gamma}{\nu}=\frac{L}{4rH_B a_p\nu}. \tag{14}$$

The problem on the particle scale is now defined. To predict the radial saturation mean defined by Eq. 10, it is necessary first to find the film thickness on one blade and then to calculate the average film thickness, $\bar{h}$, required by Eq. 1. Since the flow regime of actual films, if they exist, is unknown, it is desirable for $h(x)$ to allow for both laminar and turbulent flow, and for a general flow regime between the entry and the fully developed one. Unfortunately, the falling film problem does not have analytical solutions for all these cases, and we based the prediction of $\langle\beta\rangle$ on the limiting regimes of entry and developed flow, as was done in Buchanan's (1967) model. Figure 2b shows the entry and developed regime. At the joint between each blade and the previous one, the flow direction is suddenly changed and a loss of kinetic energy and a decrease of liquid speed occur. Immediately downstream of the joint viscosity forces are unimportant, and the flow is governed only by inertial and gravity forces. This is the entry flow regime, and it will prevail over the entire blade (Figure 2b left) under conditions at which dissipative forces are unimportant, for example, at low rotational speeds and high liquid flow rates. In principle, entry flow can be both laminar and turbulent (Bertschy et al., 1983, mention having observed turbulent entry

flow), but this is unimportant, because in the limiting entry regime only inertial forces oppose the centrifugal force (gravity in conventional packed beds). Dissipative forces, be they laminar or turbulent, are negligible. Such flow is potential and we assume also that it is one-dimensional, as has been done often in the study of falling films (Haugen, 1968; Andersson and Ytrehus, 1985). The resulting particle-scale problem is shown in Figure 2b-left. Liquid velocity on the $k$th blade in the blade chain, counting from the bed inlet, is given by the following expression:

$$u_e^{(k)^2}(x) = u_{e,i}^{(k)^2} + 2g_x^{(k)} x \cos\theta^{(k)}. \tag{15}$$

$g_x^{(k)}$ denotes the centrifugal acceleration, $r^{(k)}\omega^2$, and indices $e$ and $i$ the entry regime and initial value, respectively. Initial liquid speed $u_{e,i}^{(k)}$ is determined by the final value on the preceding blade, $u_{e,f}^{(k-1)}$, and the loss of kinetic energy at the joint. Following Buchanan (1967), we quantify this loss by Bernoulli's equation written between the points $x = d_b$ on blade $k-1$ and $x=0$ on blade $k$:

$$\frac{1}{2}\rho u_{e,f}^{(k-1)^2} = \frac{1}{2}\rho u_{e,i}^{(k)^2}(1+f). \tag{16}$$

$f$ denotes the factor of energy loss ("head loss coefficient"), which can be assigned the physical meaning of packing shape factor on the basis of the analogy between facet joints and contact points of packing elements. Equations 15 and 16 give rise to a stochastic model which can be solved for film thickness only under certain simplifications. These were explained by Bašić (1992), and we present here only the final result. The radial mean holdup in the limit of entry flow, $\epsilon\langle\beta\rangle_e$, is given by:

$$\epsilon\langle\beta\rangle_e = \xi a_p d_p \overline{Fr}_e^{1/2}, \tag{17}$$

where $\xi$ depends only on the constant $f$ from Eq. 16, and represents the final form of the adjustable packing shape factor. $\overline{Fr}_e$ denotes the Froude number, defined as:

$$\overline{Fr}_e = \left[\frac{\Gamma^2}{g d_p^3}\right]_{r=\bar{r}_e}, \tag{18}$$

in which $\Gamma$ and $g$ are to be evaluated at the mean radius $\bar{r}_e$ defined in the list of notation.

Turning now to the other limiting regime, the developed flow, we refer again to Figure 2b. On a single facet this regime is approached asymptotically downstream, as liquid accelerates under the effect of the centrifugal force (gravity in conventional packed beds). Far enough from the joint the centrifugal force (gravity) is opposed only by the dissipative forces due to viscosity or turbulence. However, the film will be in this regime over the entire blade (Figure 2b right) when dissipative forces are strong, thus, for example, at high rotational speeds and low liquid flow rates. Film thickness may then be taken as constant along one blade, but as varying from blade to blade because of variable centrifugal acceleration, $g_x = r\omega^2 \cos\theta$. To describe this film thickness of fully developed films, allowing for both laminar and turbulent flow, we use the formula given in Table 1. By setting the constants $B$ and $m$ to $\sqrt{3}$ and 1/2, respectively, this formula reduces to Nusselt's (1916) analytical solution for developed laminar films, and other values of the pair $(B,m)$ correspond to the empirical correlations for turbulent flow, as listed. Then, averaging film thickness $h_a$ over all blades gives the mean film thickness $\bar{h}$, and by using Eqs. 1 and 10, we obtain the prediction of radial mean holdup in the limit of developed flow:

$$\epsilon\langle\beta\rangle_a = 1.339 B^{2/3} a_p d_p \left(\frac{\overline{Re}_a^{2m}}{\overline{Ga}_a}\right)^{1/3}. \tag{18}$$

$\overline{Re}_a$ and $\overline{Ga}_a$ denote the Reynolds and Galileo number, respectively, evaluated at the mean radius $\bar{r}_a$, defined in the list of notation.

We expect the asymptotic predictions $\langle\beta\rangle_a$ and $\langle\beta\rangle_e$ to agree best with experimental data collected at conditions corresponding to developed and entry flow, respectively. Provided that values of the pair $(B,m)$ are chosen only from Table 1, agreement in the developed regime would indicate that the flow is laminar or turbulent, obeying a particular correlation for film thickness from the literature. To achieve agreement at conditions of entry flow, it is necessary to fit the constant $\xi$ to the data for every packing type. About the intermediate conditions we can say only that the observed dependence of $\langle\beta\rangle$ on the main operating parameters should stay within the brackets set by Eqs. 17 and 18. To find these limits we compare the model to the empirical form $\langle\beta\rangle \propto L^{m_L}\omega^{m_\omega}\nu^{m_\nu}$, and calculate the limiting values of the exponents by inspection of Eqs. 17 and 18. The results are listed in Table 2.

**Table 2. Predicted Ranges of Exponents in $\langle\beta\rangle \propto L^{m_L}\omega^{m_\omega}\nu^{m_\nu}$**

| Developed | | Entry |
|---|---|---|
| 1/3 | $\leq m_L \leq$ | 1 |
| −2/3 | $\geq m_\omega \geq$ | −1 |
| 1/3 | $\geq m_\nu \geq$ | 0 |

## Experimental Method

The model which we used to relate the bed resistance to its liquid saturation is based on the tortuosity of a packed bed. We define this quantity first, then derive the working equations and explain the measurement procedure.

### *Theory*

We first consider some simple models of porous media consisting of a nonconducting solid matrix and a void space that can be partially or completely filled with a conducting liquid. We start by developing a relation between macroscopic properties of the medium, including liquid saturation, and the conductance observed when an electrical potential difference is applied in one direction. According to the Carman-Kozeny's (Carman, 1956) model for a saturated porous medium, liquid is distributed as if filling a bundle of crooked pores, all of same length and diameter, which do not intersect and run only in one direction on the macroscopic scale. We call this direction

axial and directions perpendicular to it the transverse. Consider a sample, with length in the axial direction of $L$ and cross-sectional area $A$, of a porous medium obeying this model. If the electrical conductivity of the liquid is $\kappa_l$ and its volume fraction $\epsilon$, the sample will oppose axial conduction with resistance $R_{a,f}$, given by:

$$R_{a,f}=\frac{1}{\kappa_l}\frac{L\tau}{A\epsilon}. \tag{19}$$

$\tau$ denotes tortuosity, a model parameter to be determined experimentally for every porous medium, and subscripts $a$ and $f$ indicate the axial direction and complete saturation of the pores by the liquid, respectively. Equation 19 yields the same form for resistance as for a cylindrical conductor (or a number of them connected in parallel) of length $(L\tau)$ and (overall) cross-sectional area of $(A\epsilon)$. Hence, $\tau$ equals the ratio of the pore length to the sample length. Because no pores run in the transverse direction, resistance to transverse conduction is infinite, and an expression of the form of Eq. 19 cannot be written.

A porous medium complementary to that described by the Carman-Kozeny's model is random, isotropic and homogeneous (RIH). We call homogeneous a liquid-saturated porous medium with liquid volume fraction of $\epsilon$, obtained in the limit as the size of the largest liquid region tends to zero, while the liquid volume fraction stays equal to $\epsilon$. Further, we assume the liquid phase to be continuous, so that any two points in the liquid may be connected by a line passing entirely through the liquid. Resistance to conduction in any direction, measured on the sample described above, will be given by Eq. 19, and the ratio $(L/A)$, called cell constant, is the same in all directions. To see that, we note that the denominator of Eq. 19 again represents the fraction of the cross-sectional area available for conduction. (This follows by the so-called Dupuit's theorem, cited by Le Goff and Prost (1966) which states that when a sample of a RIH porous medium is intersected by a plane, the fraction of the section covered by any one phase equals the volume-fraction of that phase in the sample, for all directions of the section plane and all sizes of the sample.) Further, resistance is proportional to the distance between electrodes, $L$, and $\tau$ arises as the proportionality constant. Since the distribution is isotropic, the same value of resistance must be obtained by measurement in all directions of a sample with constant $(L/A)$. Tortuosity is, therefore, a constant of the particular RIH distribution, and it does not have the meaning of the pore length factor.

We assume that packed beds at complete liquid saturation can be represented by the RIH medium described above. The liquid structure may, however, take a different configuration at partial saturation, for example by forming rivulets. Anisotropy effects observed in a bed with RIH packing are, therefore, due only to liquid distribution, and may occur only at saturation below unity. As an expression for resistance in the axial (flow) or transverse direction we use again Eq. 19, replacing $(A\epsilon)$ by $(A\epsilon\beta)$:

$$R_X=\frac{1}{\kappa_l}\frac{L\tau_X}{A\epsilon\beta}, \tag{20}$$

Index $X$ denotes axial $(X\equiv a)$ or transverse $(X\equiv t)$ direction, and $R_X$ is defined as the resistance to one-dimensional conduction arising from a potential gradient in the direction $X$. The quantity $\tau_X$ denotes the still undefined tortuosity of the packed bed. Since all quantities except $\tau_X$ appearing in the above expression are measurable, we use Eq. 20 precisely as the definition of tortuosity of the packed bed in the direction $X$: it is the proportionality factor between resistance to one-dimensional conduction in direction $X$ and the quantity $L/(\kappa_l A\epsilon\beta)$. [In general, $(A\epsilon\beta)$ does not represent the liquid-covered fraction of the cross section.] Some conclusions about tortuosity of conventional packed beds can be now drawn from the experimental results summarized by Eqs. 6–8.

Considering first the axial direction $(X\equiv a)$ we set $\tau_a=\tau_a(\beta)$ for partial, and $\tau_a=\tau_{a,f}$ for full saturation. Then substituting Eq. 20 in Eqs. 6 and 7, we find that both equations are satisfied only if axial tortuosity is independent of saturation, that is when $\tau_a=\tau_{a,f}$, for all $\beta$. The experimental result for transverse resistance, Eq. 8 cannot be compared directly to Eq. 20 with $X\equiv t$ because potential distribution in Prost and Le Goff's (1964) experiment was three-dimensional. Still, a rough dependence of $\tau_t$ on $\beta$ can be recognized, because normalized conductances appearing in Eq. 8 should reflect only the effect of liquid saturation and tortuosity, and not of the cell shape. At constant saturation, the dependence of normalized resistance on tortuosity should be the same as in our one-dimensional equation, Eq. 20. Therefore, approximately $R_a/R_{a,l}\propto\tau_a$ and $R_t/R_{t,l}\propto\tau_t$, and by combining these proportionalities with Eq. 8, we find $\tau_t\propto\beta^{-0.35}$. This confirms that axial and transverse resistance of a packed bed may be described by Eq. 20, where $\tau_X$, with $X\equiv a$ or $t$, represents a parameter of liquid distribution. Moreover, $\tau_a$ is independent of saturation, therefore, a property of the packing, and $\tau_t$ decreases with the increase in saturation. Equivalently, Eq. 20 may be considered to have been derived from one-dimensional conduction in the direction $X$ through a hypothetical medium exhibiting anisotropic conductivity $(\epsilon\beta\kappa_l/\tau_X)$ with the properties described above. Since $\tau_t>\tau_a=\tau_f$ the degree of anisotropy of this medium is between those of the RIH distribution and the Carman-Kozeny's medium. We assume these conclusions to hold also for the RPB, when the flow (axial) and transfer directions of conventional packed bed are taken to correspond to flow (radial) and axial direction of the RPB, respectively.

### *Working equations*

The inset of Figure 1 shows the packed section of the rotor fitted with electrodes for radial and transverse measurements. During radial measurement, the top and bottom of the bed are isolated, and wire screens (16) are used as electrodes. In transverse measurement electrodes are thin metal sheets lining the top and the bottom of the bed (17). By isolated leads (18) electrodes of both kinds are connected to an outside circuit in which the resistance is measured. Radial and transverse resistance obtained in this way satisfy the equation:

$$R=\frac{|\Delta V|}{|I|}=\frac{|\Delta V|}{\left|\int_{A_e}\boldsymbol{i}\cdot d\boldsymbol{A}_e\right|}, \tag{21}$$

where $\Delta V$ denotes the potential difference applied between the

electrodes, $I$ the overall current, $A_e$, the surface vector of one wire screen or one plate electrode and $i$ the current density flux. The relationship between the radial and transverse resistance and liquid saturation is, therefore, determined by the distribution of current density during radial and transverse measurements. To find it, we write first the differential form of Ohm's law:

$$i = \kappa \cdot \nabla V. \tag{22}$$

where we treat the packing as a pseudo-homogeneous conductive medium, whose effective conductivity is described by the second-order tensor $\kappa$. Since the potential appears in Eq. 22 as the second unknown, one more equation is necessary, and it is supplied by conservation of charge in the absence of electrochemical reactions:

$$\nabla \cdot (\kappa \cdot \nabla V) = 0. \tag{23}$$

We define the diagonal components of $\kappa$, responsible for radial and transverse conduction, applying the conclusions from the preceding section:

$$\kappa = \epsilon \beta \kappa_l \begin{bmatrix} \frac{1}{\tau_r} & 0 \\ 0 & \frac{1}{\tau_z} \end{bmatrix}. \tag{24}$$

$\tau_r$ denotes tortuosity in the radial (flow) direction, which is independent of liquid saturation, and $\tau_z$ denotes tortuosity in the transverse direction, which is an unknown function of liquid saturation and therefore of the radial position. We assume the packing to be a RIH porous medium and denote its tortuosity by $\tau_f$. Then, $\tau_r = \tau_f$ at all conditions, and $\tau_r = \tau_z = \tau_f$ at full saturation.

In cylindrical coordinates, $(r,z)$, the boundary conditions describing radial measurements consist of zero potential gradient at the isolated top and bottom of the bed, and of fixed potential at the wire screen electrodes, $V(r_i,z) = V_i$, $V(r_o,z) = 0$, $V_i$ arbitrary. With these boundary conditions Eq. 23 gives the one-dimensional potential distribution $V = V_i[1 - f(r)/f(r_o)]$, where $f(r) = \int_{r_i}^{r} (t\beta)^{-1} dt$. To find the radial resistance, $R_r$, we then calculate $i$ from Eq. 22 at either the inner or the outer wire screen electrode, substitute the result in Eq. 21, and obtain:

$$R_r = \frac{\tau_f}{2\pi\epsilon H_B \kappa_l} \int_{r_i}^{r_o} \frac{dr}{r\beta}. \tag{25}$$

Radial resistance in the liquid-full bed follows by substituting $\beta = 1$:

$$R_{r,f} = \frac{\tau_f}{2\pi\epsilon H_B \kappa_l} \ln \frac{r_o}{r_i}, \tag{26}$$

and radial saturation mean, defined by Eq. 10, equals the ratio of $R_{r,f}$ and $R_r$:

$$\langle \beta \rangle = \frac{R_{r,f}}{R_r}. \tag{27}$$

The radial saturation mean, $\langle \beta \rangle$, thus can be obtained from experiments as the ratio of the radial resistance in the liquid-full bed and at the conditions of interest. When bed porosity and liquid conductivity are known, void tortuosity, $\tau_f$, may be found from radial resistance of the liquid-full bed, according to Eq. 26.

For transverse measurements screen electrodes are removed and the bed inlet and outlet are bounded only by perforated support rings (15, Figure 1). We use boundary conditions of zero potential gradient at $r = r_i$ and $r_o$, and discuss later the error of this approximation. Boundary conditions at the electrodes are $V(r,0) = 0$ and $V(r,H_B) = V_{top}$, $V_{top}$ arbitrary. The solution of Eq. 23 then reads simply $V = (V_{top}/H_B)z$, and we obtain the expression for transverse resistance analogously to calculating the radial one. When written in the form of conductance, the result reads:

$$R_z^{-1} = \frac{2\pi\epsilon\kappa_l}{H_B} \int_{r_i}^{r_o} \frac{1}{\tau_z} \beta r dr. \tag{28}$$

Normalizing this expression by its value in the liquid-full bed, $R_{z,f}^{-1}$ which follows by substituting $\beta = 1$ and $\tau_z = \tau_f$, we obtain the transverse saturation mean, $[\beta]$:

$$\frac{R_{z,f}}{R_z} = [\beta] = \frac{2}{r_i^2 - r_o^2} \int_{r_i}^{r_o} \frac{\tau_f}{\tau_z} r\beta dr. \tag{29}$$

The first equality in Eq. 29 states that $[\beta]$ can be obtained from experiments as the ratio of transverse resistance measured in the liquid-full bed and at conditions of interest. The second equality shows that $[\beta]$ depends on transverse tortuosity, therefore, that it contains information about anisotropy. To see that, we note first that $[\beta]$ would equal the mean saturation, $\beta_V$, defined by Eq. 9, if $\tau_z$ were equal to $\tau_f$. However, $\tau_z$ depends on $\beta$, and if in this respect the RPB is similar to conventional packed beds, $\tau_z$ increases from $\tau_f$, when $\beta = 1$, to infinity as $\beta$ tends to zero. Since an increase in $\tau_z$ reflects an increasing anisotropy, the ratio $\tau_f/\tau_z$, taking values between zero and unity, may be used to quantify isotropy, if $\tau_z$ could be measured. A more convenient measure of isotropy is the ratio $([\beta]/\beta_V)$, because it is measurable and it varies between the same limits as the ratio $(\tau_f/\tau_z)$ (c.f. Eqs. 29 and 9). The difficulty that $\beta_V$ is unknown can be overcome by replacing it by $\langle \beta \rangle$, because as we show in Appendix A $\langle \beta \rangle$ does not differ numerically from $\beta_V$ by more than a few percent. Therefore, to obtain an estimate of isotropy under given experimental conditions, we take the ratio of measurements of $[\beta]$ and $\langle \beta \rangle$, and interpret values close to unity as resulting from an isotropic liquid distribution, and those close to zero as resulting from a very anisotropic one.

### *Experimental facility and measurement procedure*

A detailed description of the experimental facility and the measurement procedure was given by Bašić (1992), and we provide here only the essential explanation. Figure 1 is a cross section of the RPB unit used, drawn slightly out of scale in

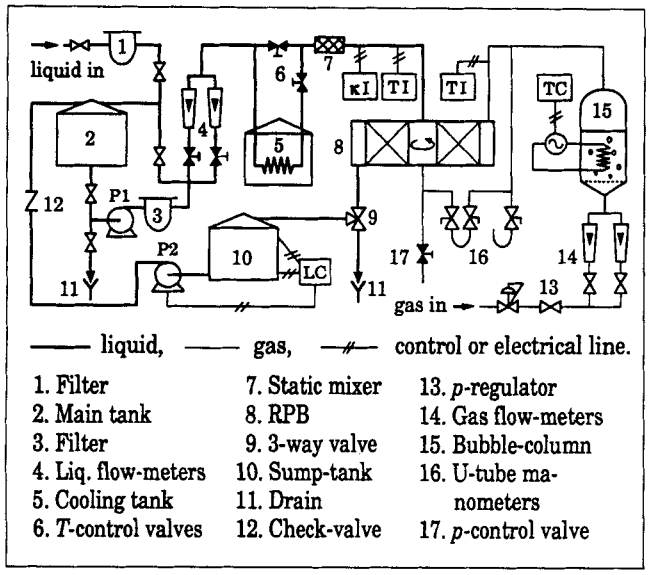


**Figure 3. Installation for liquid and gas delivery.**

order to show as much detail as possible. The distance between the bed top and bottom is 25.4 mm, and the inner and outer radius of the packed section are 31.2 and 85.4 mm, respectively. The unit is designed for maximum rotational speed of 168 rad/s (1,600 rpm). Figure 3 shows the installation for gas and liquid feed supply. In most experiments the liquid fed to the RPB (8) from the reservoir (2) was returned through the sump tank (10) and pump (P2) arrangement. Recycling was mandatory because high liquid capacity of the RPB would have made once-through operation prohibitively expensive when using solutions with controlled viscosity and surface tension. Liquid batch (2) was kept at approximately the room temperature and the heat added to the liquid by pumps P1 and P2 was removed in the cooling tank (5). Liquid temperature was measured immediately upstream of the RPB (19, Figure 1) and kept at the current room temperature by blending the cooled and uncooled portion of the incoming stream with valves (6). A bubble column (15) fitted with a heater with variable power served as the air humidifier. It enabled us to deliver air at the current room temperature and saturated at almost 100% at all flow rates, which was necessary in order to prevent transfer of sensible and latent heat between the liquid and the gas in the bed. In this way we ensured that liquid temperature and conductivity in the packed bed were the same as at the inlet to the RPB (20, Figure 1), where they were measured.

Electrodes were connected to the measurement circuit outside the RPB by isolated leads (18, Figure 1), drawn through the center of pipe (2) to the slip-ring connector (23). Two sets of rotary joints (not shown in Figure 1) allowed introducing the gas into the pipe (2) from the side, using the pipe, at the same time, as the drive-shaft. With alternating current of high enough frequency (450–500 Hz with all solutions used), the bed resistance exhibited only the ohmic component, and we obtained it by measuring the current and the potential drop across the RPB at stationary terminals (22).

In order to account for change in liquid conductivity during measurement, instead of resistances $R$ and $R_f$, we recorded the cell constant, $K$ defined as $(R\kappa_l)$. Expressing the resistances in working equations, Eqs. 27 and 29, by cell constants gives equations of equivalent form. Then, to obtain the radial saturation mean, $\langle\beta\rangle$, given by $(K_{r,f}/K_r)$, we would first find $K_{r,f}$ by measuring $R_f$ and $\kappa_l$ in a stationary bed, with rotor casing (5) and liquid delivery pipe (3) removed, and the rotor filled with tap-water. Taking care not to disturb the packing, we then covered the rotor and, operating the RPB in the usual way, measured $R_r$ and $\kappa_l$ at the conditions of interest.

The procedure for transverse measurements was slightly different. The cell constant of the liquid-full bed, $K_{z,f}$, could not be obtained by measuring $R_{z,f}$ in the way explained above for $R_{r,f}$, because the hollow in the center of the rotor would have short-circuited the top and bottom plate electrode (17, Figure 1). For this reason we had to calculate $K_{z,f}$ from Eq. 28, setting $\beta=1$ and, using the isotropy assumption, $\tau_z=\tau_f$. Then, solving Eq. 26 for $\tau_f$ and substituting it for $\tau_z$ in Eq. 28, we find:

$$K_{z,f}=\frac{2}{\ln\dfrac{r_o}{r_i}}\frac{H_B^2}{(r_i^2-r_o^2)}K_{r,f}. \tag{30}$$

After obtaining $K_{z,f}$ in this way from radial measurement in the liquid-full bed, we would empty the bed, remove the screen electrodes, install the plate electrodes, repack the bed, and measure $K_z$ in normal operation at the conditions of interest. The result, $[\beta]=K_{z,f}/K_z$, therefore, consists of two measurements between which the bed was repacked. We note the magnitude of the repacking artifact when presenting the results.

Many practical problems had to be overcome during measurements in order to make the experiments approach the assumptions of the measurement model. We mention only the most important ones. By isolating the packed section and using accurately made wire-screen electrodes (16, Figure 1), we were able to realize the boundary conditions which result in the one-dimensional potential distribution on which Eq. 27 is based. On the other hand, we could not satisfy nearly as well the boundary condition of zero potential gradient at the bed inlet, which we assumed when deriving equations for transverse measurements. The source of difficulty were the liquid jets (7, Figure 1), which shunted the packed bed with the liquid supply pipe (3, Figure 1). This makes the results of axial measurements less accurate; however, we were able to estimate the magnitude of the end-effect due to liquid jets and to show that conclusions about liquid distribution drawn from transverse measurements were conservative.

The need for nonconductive packing of a known surface area and porosity limited the choice of packing materials to nonporous glass beads with diameters of 1.1 and 3 mm. By making use of the centrifugal force, we packed the bed as densely as possible, and so reduced the artifacts of repacking and the size of regions of increased porosity next to the walls. With the larger beads, the wall effects were limited to a layer thinner than one-half of the particle diameter (1.5 mm, c.f. $H_B=25.4$ mm) and with the smaller beads they were negligible due to small size and some irregularity of shape. Thus, as could be judged by both the naked eye and by any empirical criterion for packing uniformity, packing of small glass beads could be considered a RIH medium for the purpose of interpretation of experimental data.

## Experimental Results

The values of $\langle\beta\rangle$ and $[\beta]$, which we report next in graphical

**Table 3. Distribution of Standard Deviation of Replicated Measurements of $\langle\beta\rangle$**

| % of Total No. of Means, $\overline{\langle\beta\rangle}$, with St. Dev. $s$ | 26 | 37 | 20 | 10 | 7 |
|---|---|---|---|---|---|
| $s$ (in % of $\overline{\langle\beta\rangle}$) | 0-1 | 1-2 | 2-3 | 3-4 | >4 |

form, represent the means of three to five measurements. Table 3 lists the distribution of standard deviation of replicated measurements of $\langle\beta\rangle$. Standard deviation of the transverse mean, $[\beta]$, was higher, and we report it with the results. Full tables of data were presented by Bašić (1992) and for the sake of consistency, the experiments reported on here are numbered in the same way as in that work.

### *Experiment 2: effect of liquid and gas flow rate and rotational speed*

The purpose of this experiment was to examine the dependence of $\langle\beta\rangle$ on the three main operating parameters: rotational speed, $\omega$, liquid, $L$, and gas, $G$, flow rate. Large glass beads were used and the packing properties were: $\epsilon = 0.348$, $K_{r,f} = 0.284$, and $\tau_f = 1.57$. The liquid phase was tap water with temperature between 298 and 300 K and kinematic viscosity of $9.2 \times 10^{-7}$ m$^2 \cdot$s$^{-1}$. The gas phase was humidified air at the temperature of the liquid.

Liquid flow rate and rotational speed were varied over the entire installed ranges and gas flow rate between zero and an upper limit, $G_{max}$, which depended on the values of $L$ and $\omega$. The difficulty in detecting flooding in the RPB prevented us from setting $G_{max}(L,\omega)$ at the flooding gas flow rate, as would have been logical. To detect flooding in the usual way, it would have been necessary to monitor the pressure drop across the packed section only as a function of the gas flow rate. However, only the pressure drop across the entire RPB, which is of a greater magnitude, could be measured reasonably easily. Furthermore, flooding does not occur at all points in the bed at the same time, but starts at the inner radius, where liquid saturation and gas speed are the highest. Before increased saturation spreads far enough into the bed to cause a steady rise of pressure drop, the narrow flooded ring of the packing may force the outgoing gas to flow in bubbles, disrupting and entraining the incoming liquid. In this way entrainment may occur even before flooding becomes evident. In order to determine the maximum gas flow rate consistently at all operating conditions we based it on entrainment and defined it as the value of $G$ at which 10% of the liquid fed to the rotor is entrained. The values of the liquid flow rate shown in Figure 4 are calculated as the difference between the flow rate of liquid fed to the rotor and of that entrained, the latter having been determined by collecting the liquid exiting with the gas. Measurement at conditions of high entrainment was difficult and resulted in the points with the highest standard deviation (see Table 3).

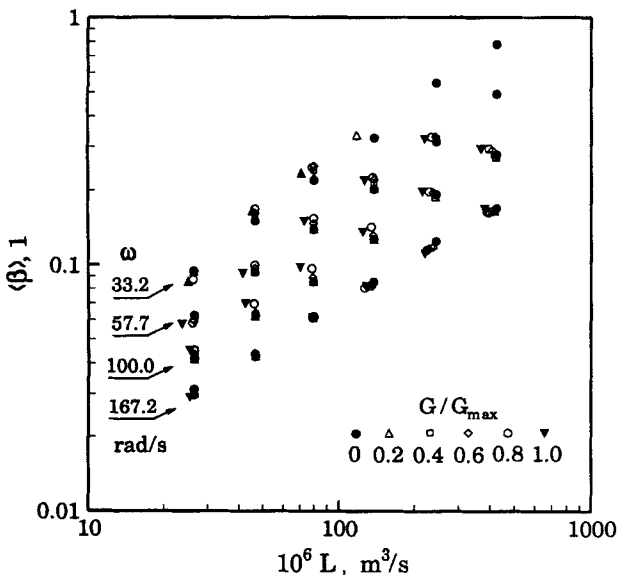


**Figure 4. Radial saturation mean as a function of gas and liquid flow rate and rotational speed.**

Figure 4 shows the results. $\langle\beta\rangle$ increases with $L$ at approximately the same rate at all levels of $\omega$, and it decreases with increase of rotational speed. The dependence of $\langle\beta\rangle$ on gas flow rate is much weaker than on $L$ and $\omega$, but several features can be distinguished. Values of $\langle\beta\rangle$ at the three uppermost points are reported only without gas flow, because at those conditions the bed was flooded even without gas flow, and passing any gas through the bed caused immediate entrainment of more than 10% of the liquid fed. Increase in gas flow rate leads first to intensified gas-liquid contact, and after that to a reduction of liquid-flow rate by entrainment. These two effects cause an increase and a decrease in liquid saturation, respectively, and their superposition may produce a minimum in variation of $\langle\beta\rangle$ with $G$. The maximum increase of $\langle\beta\rangle$ produced by varying $G$ between 0 and $G_{max}$ is about 14% of the value without gas flow. This small overall influence of gas flow rate confirms our assumption that gas flow is unimportant for liquid holdup, and we dropped the gas flow rate as a variable from further experiments.

### *Experiment 3: effect of packing size*

Figure 5 shows a comparison of $\langle\beta\rangle$ obtained with large (open symbols) and small (filled symbols) glass beads. Open symbols represent the data from the previous experiment (Figure 4) without gas flow. The properties of the bed packed with small beads were $\epsilon = 0.466$, $K_{r,f} = 0.295$, and $\tau_f = 2.26$. The pronounced increases of bed voidage and tortuosity from the values of 0.354 and 1.57, respectively, in the previous experiment were probably due to less regular shape and size of the small beads. Tap water was used as the liquid, and its temperature and kinematic viscosity were 298 K and $9.2 \times 10^{-7}$ m$^2 \cdot$s$^{-1}$, respectively.

The most pronounced effect of reducing the size of the packing was an increase in liquid saturation, which was so strong that at most points corresponding to the highest value of liquid flow rate the inner part of the rotor was flooded. For this reason we did not use the highest setting $L$ with the small beads, and solid symbols corresponding to $L$ of $423 \times 10^{-6}$ m$^3$/3 are missing from Figure 5. This still left some conditions at which the inner parts of the bed were flooded. The decrease in slope with increasing $L$, exhibited by the top line of solid points in Figure 5, illustrates this. Because local saturation

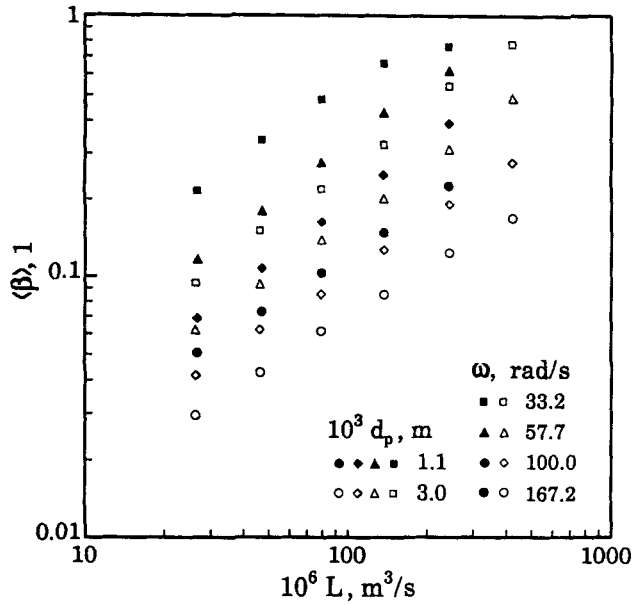


**Figure 5. Radial saturation mean with small and large glass beads.**

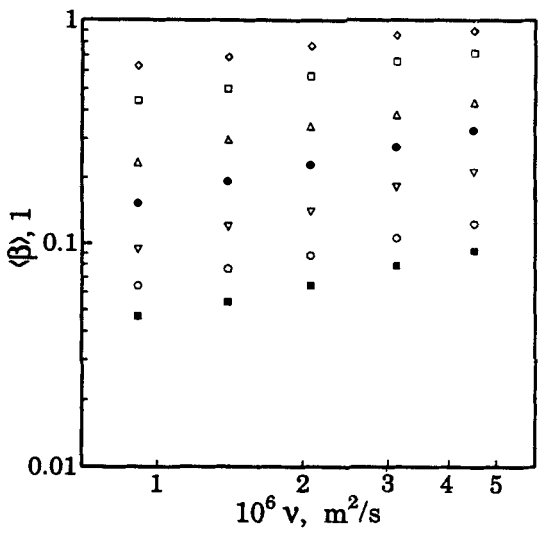


| point | $10^6$ L, $m^3/s$ | ω, rad/s | slope |
|---|---|---|---|
| ◇ | 242.5 | 57.7 | 0.23 |
| □ | 137.7 | 57.7 | 0.31 |
| △ | 137.7 | 100.0 | 0.37 |
| ◆ | 78.2 | 100.0 | 0.47 |
| ▽ | 42.5 | 100.0 | 0.51 |
| ○ | 42.5 | 167.2 | 0.41 |
| ■ | 26.6 | 167.2 | 0.44 |

**Figure 6. Radial saturation mean as a function of liquid viscosity.**

cannot exceed unity, the already fully saturated parts of the bed do not contribute to increase of $\langle\beta\rangle$ with further increase in $L$, and the overall rate of increase of $\langle\beta\rangle$ with $L$ is reduced.

To quantify the dependence of $\langle\beta\rangle$ on liquid flow rate and rotational speed, we evaluated the slopes of the best fit straight lines drawn through data points when plotted as in Figure 5, and when plotted as $\langle\beta\rangle$ vs. $\omega$ with $L$ as the parameter. The results, listed in Table 4, show that in the assumed empirical form $\langle\beta\rangle \propto L^{n_L}\omega^{n_\omega}$ absolute values of $n_L$ and $n_\omega$ change whenever a variation of any parameter causes an increase in $\langle\beta\rangle$ (such as an increase in $L$, decrease in $\omega$ and decrease in $d_p$). Superimposed on this trend is the saturation effect which reduces the rate of increase of $\langle\beta\rangle$ whenever full saturation is reached in a significant part of the bed.

### *Experiment 4: effect of liquid viscosity*

In this experiment we examined the dependence of the radial saturation mean on liquid viscosity in order to compare it to the dependence predicted by the model. $\langle\beta\rangle$ was measured using water and four solutions of propylene-glycol, which provided a range of viscosity from that of water to about 4.5 times higher. The relative density of all solutions was close to unity, but surface tension decreased with the increase of propylene-glycol concentration. There was no gas flow, and bed properties were as in the previous experiment with small glass beads. Figure 6 presents the results plotted as $\langle\beta\rangle$ vs. $\nu$, with

**Table 4. Best Fit Values of Exponents in $\langle\beta\rangle \propto L^{n_L}\omega^{n_\omega}$**

| | $n_L$ | | | | $n_\omega$ | | | | |
|---|---|---|---|---|---|---|---|---|---|
| $d_p$, | ω, rad/s | | | | $L$, $10^{-6}$ $m^3/s$ | | | | |
| mm | 33.2 | 57.7 | 100.0 | 167.2 | 26.4 | 46.3 | 79.4 | 137.6 | 243.5 |
| 1.1 | 0.59 | 0.77 | 0.79 | 0.68 | −0.91 | −0.95 | −0.96 | −0.93 | −0.76 |
| 3.0 | 0.76 | 0.74 | 0.68 | 0.63 | −0.72 | −0.77 | −0.80 | −0.83 | −0.91 |

$(L,\omega)$-pair as the parameter. The values of liquid flow rate and rotational speed were chosen so as to produce a wide range of $\langle\beta\rangle$ values. As an empirical measure of the rate of dependence of $\langle\beta\rangle$ on viscosity, in Figure 6, we list the slopes of the best-fit line drawn through the data points.

### *Experiment 7: isotropy*

In order to estimate the isotropy of the liquid distribution we measured the transverse saturation mean using the same packing and water at the same conditions as in the previous experiment. The results are shown in Figure 7 in the form of the isotropy ratio, $[\beta]/\langle\beta\rangle$, plotted as a function of the radial saturation mean with values of $\langle\beta\rangle$ taken from the previous experiment. Because the transverse measurement was more difficult and less reproducible than the radial, we first estimate the measurement artifacts.

The sources of deviation of $[\beta]$ from the true value were measurement error, repacking of the bed, and end-effects due to liquid jets. Measurement error is quantified by the standard deviation associated with the means $\overline{\langle\beta\rangle}$ and $\overline{[\beta]}$ obtained in replicated measurements. The standard deviation of $\langle\beta\rangle$ was below 3% for all the points shown, but that of $[\beta]$ reached 10% for one point. In order to estimate the effects of repacking, in a separate trial we measured the radial saturation mean before and after repacking the bed. The maximum deviation found in measurements with $\langle\beta\rangle$-values ranging from high to low was 10%. Remembering that in the absence of errors $\langle\beta\rangle \sim [\beta]$ (Appendix A) and accounting for the mag-

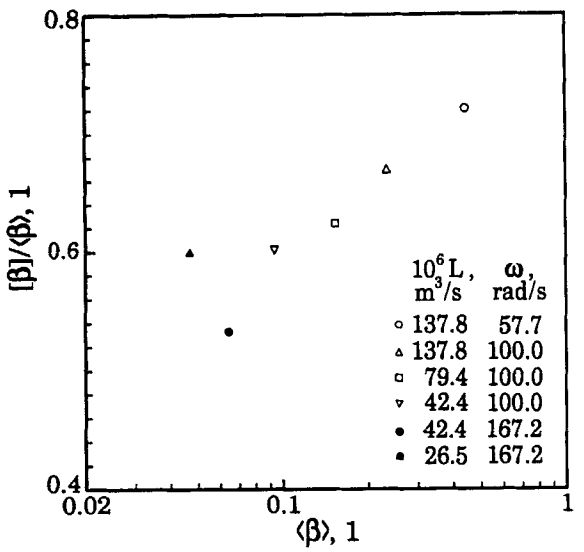


**Figure 7. Isotropy ratio as a function of the radial saturation mean.**

nitudes of the standard deviations of $\langle\beta\rangle$ and $[\beta]$ and of the errors due to repacking, it is reasonable to assume that values of $(\langle\beta\rangle - [\beta])/\langle\beta\rangle$ higher than 0.2 are due to an anisotropic distribution. The results in Figure 7 then indicate anisotropy, because the normalized difference $(\langle\beta\rangle - [\beta])/\langle\beta\rangle$ takes values between 0.27 and 0.48. Furthermore, the "isotropy-ratio," $[\beta]/\langle\beta\rangle$, exhibits an increase with the increase in saturation, $\langle\beta\rangle$. This behavior is strongly pronounced, since a straight line fit of the points in Figure 7 would represent an exponential variation of $[\beta]/\langle\beta\rangle$ with $\langle\beta\rangle$. Finally, Bašić (1992) showed that if the end-effect due to liquid jets were corrected for, the $[\beta]/\langle\beta\rangle$ ratio would indicate an even greater anisotropy.

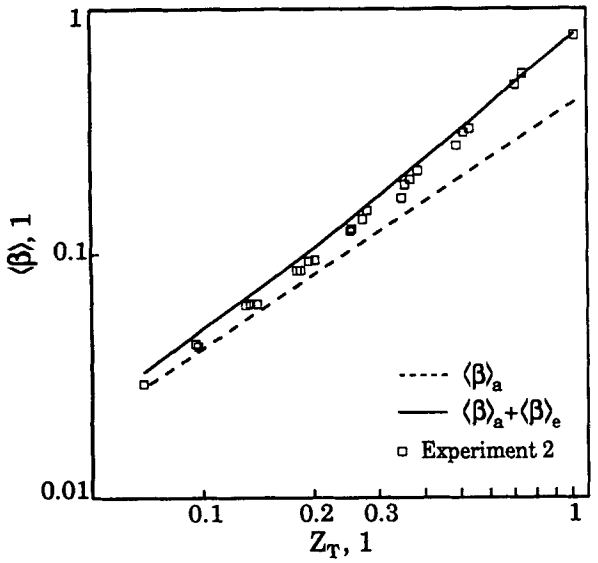


**Figure 8. Data from Experiment 2 and prediction of the model.**

$Z_T = (a_p/\epsilon)(\nu^2/\bar{g}_a)^{1/3}\overline{Re}_a^{2m/3}$, with $m = 0.875$; dashed line—$\langle\beta\rangle_a$; solid line—Eq. 31 with $\xi = 0.423$.

## Predicted and Observed Holdup

We compare first the observed and predicted rates of variation of $\langle\beta\rangle$ with operating parameters. Considering the dependence on liquid flow rate, we find that the values of the observed exponent, $n_L$, listed in Table 4, fall within the range of the exponent predicted by the model, $m_L$, given in Table 2. Moreover, $n_L$ increases with a decrease in $\omega$, and, therefore with an increase of $\langle\beta\rangle$ until the saturation effect is felt (see discussion of data in Table 4). This agrees with the behavior of the predicted exponent $m_L$, which increases as the flow regime changes from the developed one (low $\beta$) to the entry (high $\beta$). Dependence on rotational speed shows the same agreement, both in values of exponents $n_\omega$ and $m_\omega$, and in the trend of their change as liquid flow rate (therefore saturation) increases. However, the observed dependence on viscosity disagrees with the predicted one, since the slopes of data lines in Figure 6 are generally higher than the maximum value of the exponent, $m_\nu$ (Table 2) of one-third, predicted by the model for developed laminar flow. The lower slopes of the two top lines in Figure 6 are due to the saturation effect.

If, for the sake of the argument, we disregard this disagreement, we may find empirical combinations of model predictions $\langle\beta\rangle_a$ and $\langle\beta\rangle_e$, which not only fit some of the data well, but make them appear to exhibit both limiting behaviors. Figure 8 shows one example. The data are from Experiment 2 without gas flow, and the model is based on the sum of two asymptotic forms, one for entry flow, given by Eq. 17 and the other for developed flow, presented by Eq. 18:

$$\langle\beta\rangle = \langle\beta\rangle_a + \langle\beta\rangle_e = 1.339B^{2/3}\left(\frac{\nu^2}{\bar{g}_a}\right)^{1/3} Re_a^{2m/3} + \xi\overline{Fr}_e^{1/2}. \quad (31)$$

Here $B = 0.171$, $m = 0.875$, corresponding to the correlation for turbulent flow of Ganchev et al. (1972) (Table 1), $\bar{g}_a = \bar{r}_a\omega^2$, and the adjustable parameter $\xi$ is set to 0.423. (Since $Z_T$, used as the abscissa in Figure 8, is directly proportional only to $\langle\beta\rangle_a$, and not to $\langle\beta\rangle_e$, $\langle\beta\rangle$-points calculated from Eq. 31 and plotted in Figure 8 are aligned only as $Z_T \to 0$, and they are slightly scattered at higher values of $Z_T$. However, this scatter is less significant than that of the data, and the solid line in Figure 8 obtained by smoothing the model prediction represents the model well in the plane $[Z_T, \langle\beta\rangle]$.) As $Z_T$ tends to zero, the data points approach from above the asymptote $\langle\beta\rangle_a$ representing developed turbulent flow, and as $Z_T$ increases, the slopes of both the data-points and the model-line increase, reflecting a stronger dependence on $L$ and $\omega$ in the entry, than in the developed regime. Further, the data fall between the prediction for turbulent developed flow, $\langle\beta\rangle_a$, and Eq. 31, throughout the range, seemingly showing the importance of both regimes. Figure 9 compares the predictions of Eq. 31 to the analogous prediction under the assumption of laminar flow. The lower abscissa $Z_T$ and line $M_T$ are the same as the abscissa and the solid line in Figure 8, and the upper abscissa $Z_L$ and line $M_L$ are the counterparts of $Z_T$ and $M_T$, obtained by assuming laminar flow. The scatter of the experimental data plotted as solid squares against $Z_L$, relative to the alignment of the open ones, plotted against $Z_T$, seems to be the definite proof of turbulent films. However, the fallacy of this conclusion becomes apparent under scrutiny. Comparing the film thickness predicted by the model at any one set of op-

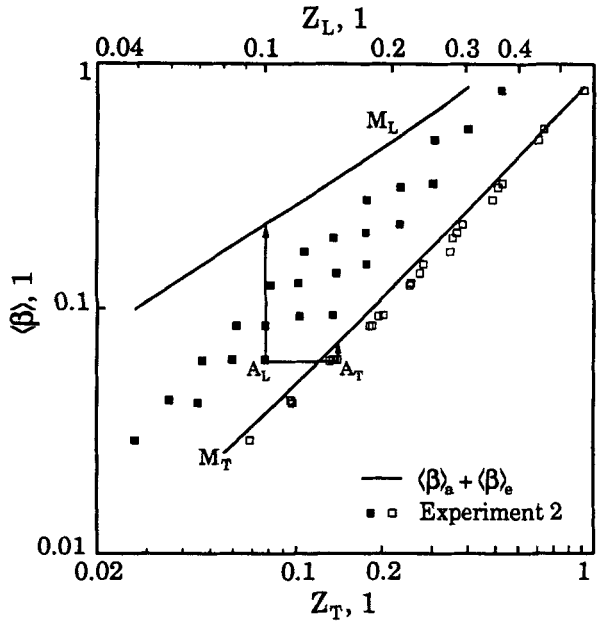


**Figure 9. Data from Experiment 2 and model predictions assuming laminar and turbulent films.**

$Z_T$ is defined as in Figure 8; $Z_L = (a_p/\epsilon)(\nu^2/\bar{g}_a)^{1/3}\overline{Re_a^{2m/3}}$, with $m = 0.5$; lines $M_L$ and $M_T$ are predictions by Eq. 31 with $\xi = 0.423$ and assuming laminar and turbulent films, respectively; solid squares—$\langle\beta\rangle_{exp}$ vs. $Z_L$; open squares—$\langle\beta\rangle_{exp}$ vs. $Z_T$.

erating parameters, such as at points $A_T(Z_T,\langle\beta\rangle)$ and $A_L(Z_L,\langle\beta\rangle)$, we see that the assumption of turbulent flow results in a lower thickness than the laminar flow assumption. This implication that at the same conditions the films would be thinner if turbulent violates the momentum balance of film flow. It also shows that Eq. 31 represents no more than a fit, and that it proves nothing about the existence of films.

The results of transverse measurements provide further evidence against the film assumption. If films covered the packing surface fully and equally in all directions, liquid would be distributed as isotropically as the packing. However, transverse measurements indicate anisotropy, which increases with decrease in liquid saturation. If we relax the assumption of ideal liquid films with complete particle wetting, we may allow, for example, for films which form preferentially on facets parallel to the radial direction, as the direction of the main body force. That would be a plausible explanation for anisotropy, and it might even go some way towards explaining the trend of decrease in isotropy with decrease in saturation. However, this can still not reconcile the model and the data, since the rates of variation of radial saturation mean with operating conditions would still be determined by the thickness of the radially oriented films, and we saw that the observed variation of $\langle\beta\rangle$ cannot be explained by any form of film flow.

The disagreement of the model and experimental results shows that a formula for liquid holdup based on the film flow model, such as Eqs. 18 or 17, or any empirical combination of them, such as Eq. 31, would have no physical basis. A theoretically meaningful equation would have to be based on a different assumption and to account for the observed anisotropy of liquid distribution. In the absence of such theory we propose an empirical formula for $\langle\beta\rangle$, in order to correlate the experimental results with the operating conditions.

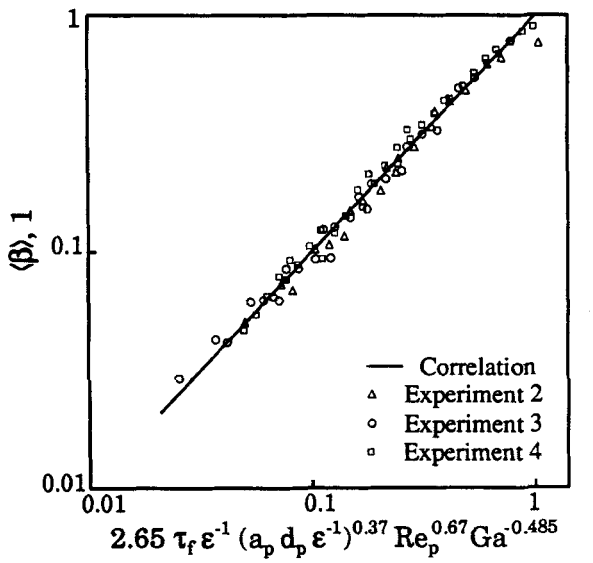


**Figure 10. Correlation of results for radial saturation mean by Eq. 32.**

### *Correlation for radial saturation mean*

If correlations for holdup in conventional packed beds in the low interaction regime are used to predict the radial saturation, a mean relative error of about 100 to 300% is obtained. However, the trends are roughly correct and while some correlations overpredict the data, others underpredict them. Thus, the often used correlations of Otake and Okada (1953) and Specchia and Baldi (1977), which are of similar form, bracket the data from below and above, respectively (Bašić, 1992). We tried to improve the fit by using an expression of the same form, but with different parameters. While this was possible to do reasonably well with the data obtained either with the small or with the large glass beads, the fits became much poorer whenever the data for both packing sizes were included. Recalling that changing the packing from large to small beads was accompanied by a marked increase of tortuosity and of liquid saturation (Experiment 3), we assumed that $\epsilon\langle\beta\rangle \propto \tau_f$, and obtained the following fit:

$$\epsilon\langle\beta\rangle = 2.65\tau_f\left(\frac{a_p d_p}{\epsilon}\right)^{0.37} Re^{0.67} Ga^{-0.485} \qquad (32)$$

whose maximum discrepancy with respect to the data is 9%. Figure 10 shows the agreement in graphical form. The parameter $\tau_f$ must be found experimentally for every packing type.

## Discussion and Conclusions

The data for the radial saturation mean reported here represent the first results for holdup of RPBs. They allowed us to test the film flow assumption, and we found that holdup cannot be predicted on the basis of film flow on the particle scale. The results indicate further that liquid is connected better

in the radial than in the transverse direction, suggesting flow in the form of radially oriented rivulets, rather than isotropically distributed films. This leads us to conclude that mass-transfer models, which were based on the film flow assumption (Tung and Mah, 1985; Munjal et al., 1989a,b) do not have a strong physical basis. This certainly does not diminish the usefulness of expressions for mass-transfer coefficients, which are reported in these studies and are shown to agree with experimental data. However, these expressions should not be given more significance than empirical correlations.

Equation 32 correlates well the measured radial saturation mean with operating parameters. It has the form of correlations for holdup of conventional packed beds in the regime of low gas-liquid interaction, therefore, without a dependence on gas flow rate, but with a dependence on tortuosity of the liquid-full bed, $\tau_f$.

We have used the term film flow for a flow regime with either complete wetting, or one in which the mean film thickness, $\bar{h}$, and not the wetted area, $a_\omega$, determines local saturation, $\beta$, (c.f. Eq. 1). Let us consider what the assumption of film flow with substantially incomplete wetting would imply for a future model. When this is allowed, we may ascribe the observed behavior of liquid holdup to the wetted area, rather than to film thickness. Indeed, all film flow models for conventional packed beds, except that of Bemer and Kalis (1978), were corrected on account of unknown wetted area. However, when this is done agreement between a holdup prediction and holdup data cannot be taken as evidence of liquid films. In order to show by a physical model that liquid flows in the form of films which wet the packing surface partially, it would be necessary to predict the wetted area, $a_\omega$, of such film flow on the particle scale. Unfortunately, this proposition is hardly practical. Film flow with partial wetting is governed by the capillary force between the liquid and the solid, and it is not probable that films with partial wetting similar to those on flat inclines (such as Hartley and Murgatroyd, 1964) are established on the irregular packing surface. Our results for anisotropy indicate, on the contrary, that patterns of wetted and nonwetted regions of packing are formed on a scale larger than the particle scale. When the liquid phase takes this form, it cannot be said to flow in the form of films. In short, the assumption of film flow, with complete wetting or otherwise, is not a practical basis for description of the hydrodynamics of the RPB.

Our measurement method is based on tortuosities in the direction of flow and in the transverse direction as the key quantities. We defined them in order to quantify the largely qualitative results from previous studies of conventional packed beds, which suggested that the axial and transverse direction were the principal ones for describing liquid distribution. Invoking analogy with conventional packed beds, we then assumed only that radial tortuosity was a constant, with the transverse one dependent on liquid saturation, and we obtained the expressions for measured quantities, radial and transverse saturation mean. We showed further than the first one was a good measure of overall liquid saturation, and the second of the isotropy of liquid distribution. Theoretically, it is possible to obtain more information by measuring resistance in more directions, and even to find distributions of local voids saturation and of both tortuosities. However, this amounts to resistance tomography and in any system, particularly in the RPB, that is a difficult experiment to carry out (Webster, 1990). Our goal was achieved by a much simpler measurement.

The limitations of the measurement method in this study were imposed by the geometry and construction of the RPB. The resistance technique may be exploited more fully for characterizing liquid distribution in conventional packed beds, which are not beset by the practical problems of the RPB, and in which holdup can be measured independently. This is not a new idea, but its potential has been underestimated. In the best known experimental study in which this principle was employed, Charpentier et al. (1968) (see also Le Goff, 1967) used measurements of liquid holdup and of resistance in two directions to determine three parameters of a model of liquid distribution in packed beds. The model described liquid as a regular lattice of unit cells with three structural elements, assumed equivalent to rivulets, films and liquid drops in the packed bed. The volume fraction of liquid in the bed under each one of these forms was then found by comparing the three experimental results with model predictions. The triangular plots of the fraction of liquid as films, rivulets and drops, which these authors reported, are regarded as the only contribution so far towards description of liquid structure in packed beds. However, these results are interpretation of the resistance data in terms of an assumed structure, and a regular one. We do not think that liquid distribution can be described in terms of such a model. Liquid flow through a packed bed is a complex process, and there is no reason to assume that it may be described by phenomena on the particle scale, as the film flow models assume, or as a regular lattice of a hypothetical structural unit, as Charpentier et al. (1968) assumed. Instead, sensitivity and reproducibility of resistance measurements, demonstrated by Charpentier et al. (1968) and in this work (c.f. Table 3), should be exploited to gather experimental data describing liquid flow and distribution on the bed scale. Treating the liquid as a phase of a porous medium and characterizing its distribution by tortuosity is just one possibility.

## Acknowledgment

This work was funded by the NSF grant no. CBT-8709760 and by the Industrial Participants of the Chemical Reaction Engineering Laboratory (CREL). Thanks are due to: Dr. Henry F. Erk, Dr. William F. Pickard, Washington University's Instrument Shop, Gene Bulfin, Dr. Norbert Mason, Chris McCann, David Bartels, Paul Lincoln, and Steve Picker.

## Notation

$a$ = surface area of the packing per unit volume of the bed
$A$ = area of the bed section perpendicular to flow
$d$ = diameter of the packing particle
$g$ = gravitational or centrifugal acceleration
$G$ = volumetric flow rate of the gas
$H_B$ = packing height in the RPB
$f$ = energy loss factor, Eq. 16
$L$ = volumetric flow rate of the liquid
$m$ = constant in Tables 1 and 2
$n$ = constants in Table 4
$\bar{r}_a$ = mean radius for developed flow; $\bar{r}_a^{(2m+1)/3} = [r_o^{(2m+1)/3} - r_i^{(2m+1)/3}]/\ln(r_o/r_i)^{(2m+1)/3}$
$\bar{r}_e$ = mean radius for entry flow; $\bar{r}_e^{3/2} = (r_o^{3/2} - r_i^{3/2})/\ln(r_o/r_i)^{3/2}$
$R$ = electrical resistance
$Re_p$ = particle Reynolds number, $Ld_p/(A_B\nu)$
$s$ = standard deviation of measurement
$S$ = conductance, $R^{-1}$
$V$ = volume; electrical potential

$X$ = hydrodynamic entry length
$Z$ = abscissas in Figures 8 and 9

### Greek letters

$\beta_V$ = mean saturation of the RPB, Eq. 9
$\langle\beta\rangle$ = radial saturation mean of the RPB, Eq. 10
$[\beta]$ = transverse saturation mean of the RPB, Eq. 29
$\theta$ = angle of inclination relative to the radius; tangential direction
$\kappa$ = electrical conductivity
$\nu$ = kinematic viscosity of the liquid
$\xi$ = packing shape factor, Eq. 17
$\sigma$ = surface tension of the liquid

### Subscripts and superscripts

$a$ = in the axial (flow) direction; asymptotic at $\bar{r}_a$
$b$ = of the rotating blade
$B$ = of the packed bed
$e$ = in entry flow; at $\bar{r}$
$f$ = in liquid-full bed; at $x = d_b$
$i$ = at the inlet; at the leading edge
$l$ = with liquid as the only phase
$lm$ = laminar flow
$o$ = at the bed outlet
$pt$ = in potential flow
$r$ = in the radial direction
$t$ = in the transverse direction
$u$ = $x$-component of liquid velocity
$x$ = flow direction on the rotating blade
$z$ = axial direction of the RPB
$\bar{}$ = mean value
$^*$ = characteristic value

## Literature Cited


Achwal, S. K., and J. B. Stepanek, "An Alternative Method of Determining Liquid Hold-up in Gas-Liquid Systems," *Chem. Eng. Sci.*, **30**, 1443 (1975).

Andersson, H. I., and T. Ytrehus, "Falkner-Skan Solution for Gravity-Driven Film Flow," *J. Appl. Mech.*, **52**, 783 (1985).

Bard, A. J., and L. R. Faulkner, *Electrochemical Methods*, Wiley, New York (1980).

Bašić, A., *Liquid Holdup and Hydrodynamics of Rotating Packed Beds*, D. Sc. Diss., Washington Univ., St. Louis (1992).

Belkin, H. H., A. A. McLeod, C. C. Monard, and R. R. Rothfus, "Turbulent Liquid Flow Down Vertical Walls," *AIChE J.*, **5**, 245 (1959).

Bemer, G. G., and G. A. J. Kalis, "A New Method to Predict Hold-up and Pressure Drop in Packed Columns," *Trans. Inst. Chem. Eng.*, London, **56**, 200 (1978).

Bertschy, J. R., R. W. Chin, and F. H. Abernathy, "High-Strain-Rate Free-Surface Boundary-Layer Flows," *J. Fluid Mech.*, **126**, 443 (1983).

Blok, J. R., and A. A. H. Drinkenburg, "Hydrodynamic Properties of Pulses in Two-Phase Downflow Operated Packed Columns," *Chem. Eng. J.*, **25**, 89 (1982).

Brauer, H., "Strömung und Wärmeübergang bei Rieselfilmen," *VDI Forschungsheft*, 457 (1956).

Brötz, W., "Über die Vorausberechnung der Absorptionsgeschwindigkeit von Gasen in strömenden Flüssigkeitsschichten," *Chem. Ing. Tech.*, **26**, 470 (1954).

Buchanan, J. E., "Holdup in Irrigated Ring-Packed Towers below the Loading Point," *Ind. Eng. Chem. Fund.*, **6**, 400 (1967).

Buchanan, J. E., "Operating Holdup on Film-Type Packings," *AIChE J.*, **34**, 870 (1988).

Carman, P. C., *Flow of Gases through Porous Media*, Butterworths, New York (1956).

Cerro, R. L., and S. Whitaker, "Entrance Flows with a Free Surface: the Falling Liquid Film," *Chem. Eng. Sci.*, **26**, 785 (1971).

Charpentier, J.-C., C. Prost, W. Van Swaaij, and P. Le Goff, "Etude de la Rétention de Liquide dans une Colonne à Garnissage Arrosé à Co-courant et à Contre-Courant de Gaz-Liquide," *Chimie et Industrie-Génie Chimique*, **99**, 803 (1968).

Crine, M., and P. Marchot, "Measuring Dynamic Liquid Holdup in Trickle-Bed Reactors under Actual Operating Conditions," *Chem. Eng. Commun.*, **8**, 365 (1981).

Davidson, J. F., "The Hold-up and Liquid Film Coefficients of Packed Towers: II. Statistical Models of the Random Packing," *Trans. Inst. Chem. Eng.*, London, **37**, 131 (1959).

Duduković, M. P., "Tracer Methods in Chemical Reactors. Techniques and Applications," in *Chemical Reactor Design and Technology*, H. I. de Lasa, ed., NATO ASI Ser. E: No. 110, Nijhoff (1986).

Feind, K., "Strömungsuntersuchungen bei Gegenstrom von Rieselfilmen und Gas in lotrechten Rohren," *VDI Forschungsheft*, 481 (1960).

Fowler, R., "HIGEE-A Status Report," *Chem. Eng. (London)*, 456, 35 (1989).

Ganchev, B. G., V. M. Kozlov, and V. V. Lozovetskiy, "A Study of Heat Transfer to a Falling Fluid Film at a Vertical Surface," *Heat Trans. Sov. Res.*, **4**, 102 (1972).

Gimbutis, G. J., "Heat Transfer in a Turbulent Vertically Falling Film," *Proc. Int. Heat Trans. Conf.*, Tokyo, **2**, 85 (1974).

Gimbutis, G. J., A. J. Drobavičius, and S. S. Šinkunas, "Heat Transfer of a Turbulent Water Film at Different Initial Flow Conditions and High Temperature Gradients," *Proc. Int. Heat Trans. Conf.*, Toronto, **1**, 321 (1978).

Hartley, D. E., and W. Murgatroyd, "Criteria for the Breakup of Thin Liquid Layers Flowing Isothermally Over Solid Surfaces," *Int. J. Heat and Mass Trans.*, **7**, 1003 (1964).

Haugen, R., "Laminar Flow Along a Vertical Wall," *J. Appl. Mech.*, **35**, 631 (1968).

Henstock, W. H., and T. J. Hanratty, "The Interfacial Drag and the Height of the Wall Layer in Annular Flows," *AIChE J.*, **22**, 990 (1976).

Keyvani, M., and N. C. Gardner, "Operating Characteristics of Rotating Beds," *Chem. Eng. Prog.*, **85**, 48 (1989).

Kumar, P. M., and D. P. Rao, "Studies on a High-Gravity Gas-Liquid Contactor," *Ind. Eng. Chem. Res.*, **29**, 917 (1990).

Larkins, R. P., R. P. White, and D. W. Jeffrey, "Two-Phase Co-current Flow in Packed Beds," *AIChE J.*, **7**, 231 (1961).

Le Goff, P., and C. Prost, "Interprétation de la Conductivité et de la Diffusivité Apparentes des Milieux Poreux et Dispersés à l'Aide de Modèles Géométriques à Cellules Cubiques," *Chimie et Industrie-Génie Chimique*, **95**, 1 (1966).

Le Goff, P., "Geometric Problems in the Study of Porous Media. Application to Gas-Liquid Packed Columns," Davis-Swindin Memorial Lecture, Loughborough Univ., England (1967).

Mersmann, A., H. Voit, and R. Zeppenfeld, "Brauchen wir Stoffaustausch-Maschinen?," *Chemie-Ingenieur-Technik*, **58**, 87 (1986); "Do We Need Mass Transfer Machines?," *Int. Chem. Eng.*, **28**, 1 (1988).

Munjal, S., M. P. Duduković, and P. A. Ramachandran, "Mass Transfer in Rotating Packed Beds: I. Development of Gas-Liquid and Liquid-Solid Mass-Transfer Coefficients," *Chem. Eng. Sci.*, **44**, 2245 (1989a).

Munjal, S., M. P. Duduković, and P. A. Ramachandran, "Mass Transfer in Rotating Packed Beds: II. Experimental Results and Comparison with Theory and Gravity Flow," *Chem. Eng. Sci.*, **44**, 2257 (1989b).

Nusselt, W., "Die Oberflächenkondensation des Wasserdampfes," *Zeitschrift des VDI*, **60**, 541 (1916).

Otake, T., and K. Okada, "Liquid Holdup in Packed Towers," *Kagaku Kogaku*, **17**, 176 (1953).

Prost, C., "Etude des Fluctuations de la Texture Liquide s'Écoulant à Contre-Courant ou à Co-currant de Gaz dans une Garnissage de Colonne d'Absorption," *Chem. Eng. Sci.*, **22**, 1283 (1967).

Prost, C., and P. Le Goff, "Etude, par Conductivité Électrique, de Filets Liquides Coulant dans une Colonne à Garnissage avec Contre-Courant ou Co-courant de Gaz," *Chimie et Industrie-Génie Chimique*, **91**, 6 (1964).

Ramshaw, C., "HIGEE Distillation—An Example of Process Intensification," *Chem. Eng. (London)*, 389, 13 (1983).

Ramshaw, C., and R. H. Mallinson, United States Patent No. 4283255 (1981).

Specchia, V., and G. Baldi, "Pressure-Drop and Liquid Holdup for Two-Phase Concurrent Flow in Packed Beds," *Chem. Eng. Sci.*, **32**, 515 (1977).
Takahama, H., and S. Kato, "Longitudinal Flow Characteristics of Vertically Falling Liquid Films without Concurrent Gas Flow," *Int. J. Multiphase Flow*, **6**, 203 (1980).
Tung, H. H., and R. S. H. Mah, "Modeling of Liquid Mass Transfer in HIGEE Separation Process," *Chem. Eng. Commun.*, **39**, 147 (1985).
Vivian, J. E., P. L. T. Brian, and V. J. Krukonis, "The Influence of Gravitational Force on Gas Absorption in a Packed Column," *AIChE J.*, **11**, 1088 (1965).
Wammes, W. J. A., S. J. Mechielsen, and K. R. Westerterp, "The Influence of Pressure on the Liquid Hold-Up in a Co-Current Gas-Liquid Trickle-Bed Reactor Operating at Low Gas Velocities," *Chem. Eng. Sci.*, **46**, 409 (1991).
Webster, J. G., ed., *Electrical Impedance Tomography*, Adam Higler (1990).
Yilmaz, T., and H. Brauer, "Beschleunigte Strömung von Flüssigkeitsfilmen an ebenen Wänden und Füllkörperschichten," *Chemie-Ingenieur-Technik*, **45**, 928 (1973).

## Appendix A: Comparison of Different Saturation Means

Since the actual distribution of local saturation in the RPB, $\beta(r)$, is unknown, it is possible to compare the values of $\langle\beta\rangle$ and $\beta_V$, defined by Eqs. 25 and 9, respectively, only using an arbitrarily chosen $\beta(r)$. We set $\beta \propto r^{-n}$, and by varying the value of $n$ we examine the dependence of the means $\beta_V$ and $\langle\beta\rangle$ on the rate of change of $\beta$ with the radius. Setting $\beta_i = \beta(r_i)$, where $\beta_i$ is an unknown constant equal to local saturation at the bed inlet, we have $\beta = \beta_i (r/r_i)^{-n}$ and $\langle\beta\rangle/\beta_i = (u^n - 1)^{-1} \ln u^n$, for all $n$, where $u = r_o/r_i$. Thus, for the assumed form of $\beta_i$, the ratio $\langle\beta\rangle/\beta_i$ equals the logarithmic mean difference of $(r/r_o)^n$ evaluated at $r = r_o$ and at $r_i$. Further, $\beta_V/\beta_i = 2(u^{n+2} - 1)/[(n+2)(u^2 - 1)]$ for $n \neq 2$, and $\bar{\beta} = \langle\beta\rangle$ for $n = 2$. Figure A1 shows the normalized profile $\beta(r)/\beta_i$ and normalized means $\langle\beta\rangle/\beta_i$ and $\beta_V/\beta_i$ calculated for our bed ($r_o/r_i = 2.72$) and with 0.5, 1 and 2 for the value of power $n$. For all three values of power $n$, the two means differ by less than 5% and the value of $\langle\beta\rangle$ corresponds to some local value of $\beta$ close to the midpoint of the bed. This does not prove, but suggests strongly that the value of radial saturation mean $\langle\beta\rangle$ is very close in value to that of the mean saturation $\beta_V$ for all realistic profiles $\beta(r)$.

## Appendix B: Magnitude of Body Forces in the RPB

If by $U_r^*$ and $U_\theta^*$ we denote the characteristic liquid speed in the radial and tangential direction, respectively, and by $\bar{r}$ some mean radial position, such as the arithmetic mean, characteristic values of body forces per unit liquid mass are $U_r^* U_\theta^*/\bar{r}$ for the Coriolis and $U_\theta^{*2}/\bar{r}$ for the centrifugal. The ratio of these two quantities equals $U_r^*/U_\theta^*$ and can be taken as a measure of the relative importance of the Coriolis to the centrifugal force. We set $U_\theta^* = \bar{r}\omega$, assuming that the lag of tangential liquid speed relative to the packing is of a lower magnitude than the speed itself. This situation arises whenever liquid flows over a rotating solid surface and the ratio of the solid surface area (at which tangential speed equals $r\omega$) to liquid volume (throughout which tangential speed lags $r\omega$) is high, such as in liquid films on rotating disks. On the other hand, there is no characteristic radial speed that we could use for $U_r^*$. We calculate it as the ratio of the radial span $(r_o - r_i)$ and the mean residence time $\bar{t}$, estimating $\bar{t}$ from experimental data as the ratio of liquid contents $V_B \epsilon \beta_V$ and liquid flow rate $L$. In this way, $U_r^* = L/(2\pi \bar{r} H_B \epsilon \beta_V)$ and

$$\frac{\text{(Coriolis force)}}{\text{(centrifugal force)}} = \frac{U_r^*}{U_\theta^*} = \frac{r_o - r_i}{\bar{t}\,\bar{r}\omega} = \frac{1}{2\pi} \frac{L}{\epsilon \bar{\beta} H_B \bar{r}^2 \omega}.$$

Since $\beta_V \approx \langle\beta\rangle$ (Appendix A), we can estimate the righthand side of the last equality for any experimental condition and the measured value of $\langle\beta\rangle$. The highest value of the ratio $U_r^*/U_\theta^*$ that occurred in the experiments was 0.15 and corresponds to the lowest point in Figure 4. In all other experiments, it had half this value at most.

The ratio of the gravitational to the centrifugal force per unit mass of liquid equals $g/(\bar{r}\omega^2)$. It varied between 0.015 at the lowest value of $\omega$ to 0.006 at the highest.

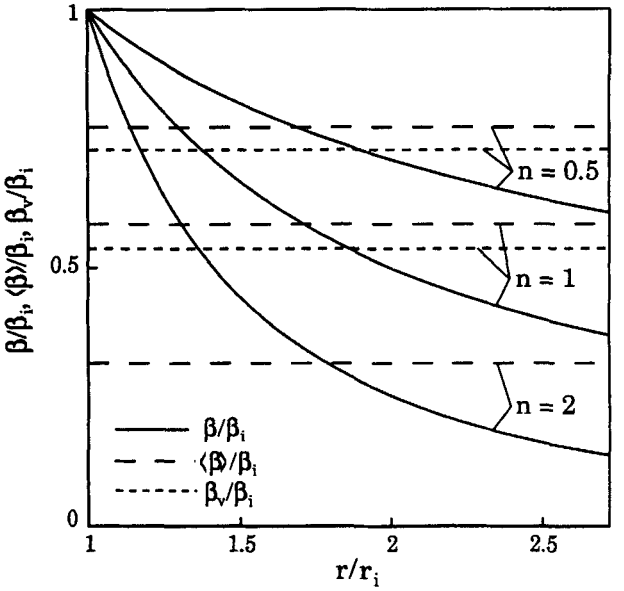


**Figure A1. Radial saturation mean, saturation mean and location saturation.**

Local saturation is assumed to be described by $(\beta/\beta_i) = (r/r_i)^{-n}$

*Manuscript received Nov. 9, 1993, and revision received Feb. 16, 1994.*